Luo *et al. Chem. Synth.* **2025**, *5*, 35
DOI: 10.20517/cs.2024.197

Chemical Synthesis

Research Article

Open Access

Check for updates

Modulating oxygen vacancies in Pt-WO_x-decorated MOF-74(Co) catalysts for the efficient conversion of glucose to 1,2-propanediol under mild conditions

Shuang Luo[#], Min Mao[#], Haijie Yu, Yuxin Zheng, Zhaohui Liu[*], Lingmei Liu[*], Jianjian Wang[*]

School of Chemistry and Chemical Engineering, State Key Laboratory of Coal Mine Disaster Dynamics and Control, Institute of Advanced Interdisciplinary Studies, Multi-scale Porous Materials Center, Chongqing University, Chongqing 401331, China.
[#]Authors contributed equally.

[*]**Correspondence to:** Dr. Zhaohui Liu, Prof. Lingmei Liu, Prof. Jianjian Wang, School of Chemistry and Chemical Engineering, State Key Laboratory of Coal Mine Disaster Dynamics and Control, Institute of Advanced Interdisciplinary Studies, Multi-scale Porous Materials Center, Chongqing University, No.55 University Town South Road, Shapingba District, Chongqing 401331, China. E-mail: zhaohui.liu@cqu.edu.cn; lmliu@cqu.edu.cn; wangjianjian@cqu.edu.cn

How to cite this article: Luo, S.; Mao, M.; Yu, H.; Zheng, Y.; Liu, Z.; Liu, L.; Wang, J. Modulating oxygen vacancies in Pt-WO_x-decorated MOF-74(Co) catalysts for the efficient conversion of glucose to 1,2-propanediol under mild conditions. *Chem. Synth.* **2025**, *5*, 35. https://dx.doi.org/10.20517/cs.2024.197

Received: 15 Dec 2024 **First Decision:** 5 Feb 2025 **Revised:** 13 Feb 2025 **Accepted:** 19 Feb 2025 **Published:** 14 Mar 2025

Academic Editor: Guangshan Zhu **Copy Editor:** Pei-Yun Wang **Production Editor:** Pei-Yun Wang

Abstract

Selective conversion of glucose to valuable 1,2-propanediol (1,2-PDO) has been a research priority, but the process often suffers from problems such as harsh reaction conditions. Therefore, the development of efficient catalysts for the efficient synthesis of 1,2-PDO from glucose under mild conditions is essential. Herein, we prepared Pt-WO_x-metal-organic framework (MOF)-74(Co) catalysts by a simple two-step method, achieving a high yield of 52.9% of 1,2-PDO under milder conditions (160 °C, 0.2 MPa H_2, 4 h), surpassing the majority of recent studies in this field. High-resolution transmission electron microscopy (HRTEM) revealed that Pt nanoparticles (~2.1 nm) and WO_x species were uniformly dispersed within the structure of MOF-74(Co). The experimental results confirmed that MOF-74(Co) facilitated the isomerization of glucose into fructose, which then underwent further conversion to yield 1,2-PDO. In addition, X-ray photoelectron spectroscopy (XPS), electron paramagnetic resonance (EPR) and NH_3 temperature-programmed desorption (NH_3-TPD) results revealed that Pt-WO_x-MOF-74(Co) has more oxygen vacancies to act as acidic sites. *In situ* diffuse reflectance infrared Fourier transform spectroscopy (DRIFTS) further confirmed the efficient conversion of glucose to intermediate and final products over Pt-WO_x-MOF-74(Co). Furthermore, cycling experiments confirmed that Pt-WO_x-MOF-74(Co) can be reused several times. This is the

first report that MOFs can be employed as the catalyst support in facilitating glucose conversion to diols, which provides important guidance for using MOFs in biomass utilization in the future.

Keywords: Biomass, MOF-74(Co), Pt nanoparticles, WO_x species, oxygen vacancies, 1, 2-propanediol

INTRODUCTION

With the depletion of traditional fossil resources, the efficient conversion of renewable biomass into liquid fuels and high-value-added chemicals has attracted widespread attention[1-4]. Among them, 1,2-propanediol (1,2-PDO) is a critical raw material for the synthesis of useful chemicals, such as surfactants, plasticizers, and surfactants, as well as a final product for applications in the pharmaceutical, food, and refrigeration industries[5,6]. Typical production methods for 1,2-PDO include petroleum product conversion, glycerol hydrogenolysis, and direct biomass hydrogenolysis[7,8]. Comparatively, the hydrogenolysis of biomass is considered to be green-friendly with sufficient bio-feedstocks such as polysaccharides (e.g., stalks and cellulose)[9] and monosaccharides (e.g., glucose and fructose)[10]. Among them, it is significant to attack the glucose conversion pathway because glucose is not only the starting material for the production of 1,2-PDO but also an important intermediate for the conversion of polysaccharide biomass to 1,2-PDO.

However, during the preparation of 1,2-PDO, glucose undergoes multiple reaction pathways [Supplementary Figure 1]. On the one hand, glucose undergoes isomerization to yield fructose, which subsequently undergoes a retro aldol condensation (RAC) to form C3 compounds such as 1,3-dihydroxyacetone and glyceraldehyde. These C3 compounds are then subjected to hydrogenation or hydrogenolysis processes, resulting in the production of 1,2-PDO and 1,3-propanediol (1,3-PDO)[11,12]. Both of them can be used as the monomers for the synthesis of polyester; however, the selectivity of 1,2-PDO is generally much higher than that of 1,3-PDO in the catalytic conversion of glucose, owing to the facile hydrogenolysis of a terminal hydroxyl group in glucose's structure[9]. On the other hand, glucose undergoes a RAC reaction to produce C2-C4 intermediates, which are then further hydrogenated at the metal site to ethylene glycol (EG), 1,2-butanediol (1,2-BDO), and 1,4-butanediol (1,4-BDO)[13-16]. Hence, enhancing the selectivity of 1,2-PDO in the hydrogenolysis process of glucose necessitates the facilitation of isomerization of the C6 sugar and the RAC reaction, concurrently minimizing the direct hydrogenation of the C6 sugars.

Since metal oxide carriers can act as electronic modulators for noble metal nanoparticles, a variety of metal oxides have been used to support noble metal nanoparticles (e.g., Ru, Pt, Pd) for selective hydrogenolysis of glucose in the aqueous phase[15,17-21]. For example, Lv *et al.* synthesized Pd@Al-$MSiO_2$ yolk-shell structured nanospheres for the catalytic preparation of 1,2-PDO from glucose, which showed a 1,2-PDO yield of 22.7% after a reaction at 200 °C, 5 MPa, for 3 h[18]. The Pd@Al-$MSiO_2$ utilized its unique core-shell structure to provide an active site for the RAC reaction of fructose. In a previous study, Gu *et al.* constructed a Pt/SiO_2@$Mg(OH)_2$ core-shell catalyst with good catalytic activity for the selective hydrogenation of glucose[17]. After a 4 h reaction period at a temperature of 180 °C and a H_2 pressure of 6 MPa, the yield of 1,2-PDO reached 53.8%. They realized the feasibility of glucose hydrogenation to 1,2-PDO by examining the base site combined with the hydrogenation site. Although the 1,2-PDO yield in this study was objective, it also reacted under high temperature and high pressure, which made the experimental conditions more stringent.

In our prior research[22], we observed that the Ru-WO_x-MgO_y efficiently facilitated the conversion of fructose into 1,2-PDO under moderate experimental conditions. However, when glucose was used as the substrate, the resulting yield of 1,2-PDO was disappointing. Therefore, we prepared Pt-WO_x-metal-organic framework (MOF)-74(Co) catalysts with MOF-74(Co) as a carrier by *in situ* synthesis for the selective

hydrogenolysis of glucose to 1,2-PDO. MOFs are a novel class of materials that have attracted much attention due to their distinctive structural and functional properties. They have been applied in a wide range of fields, especially in environmental management and energy applications[23-25]. Recently, many studies have designed MOFs-supported noble metal catalysts and shown excellent catalytic performance for biomass conversion[26,27]. However, these noble metal particles are usually dispersed on the outer surface of MOFs and can easily aggregate to some extent.

Herein, Pt-WO_x-MOF-74(Co) catalysts were facilely constructed and Pt nanoparticles (Pt NPs) (~2.1 nm) along with WO_x species were observed to be highly uniformly dispersed on the surface of MOF-74(Co) by high-resolution transmission electron microscopy (HRTEM). Employing milder reaction parameters, specifically a temperature of 160 °C, a H_2 pressure of 0.2 MPa, and a reaction time of 4 h, Pt-WO_x-MOF-74(Co) was able to fully convert glucose with a yield of 1,2-PDO as high as 52.9%. The experimental results revealed that the MOF-74(Co) catalyst enhanced the isomerization of glucose into fructose, thereby subsequently boosting the generation of 1,2-PDO. Moreover, a series of characterizations such as X-ray photoelectron spectroscopy (XPS), electron paramagnetic resonance (EPR), and NH_3 temperature-programmed desorption (NH_3-TPD) suggested that WO_x modulated the oxygen vacancies of MOF-74(Co), thereby generating additional acidic sites, which was beneficial for glucose isomerization and RAC reactions. According to *in situ* diffuse reflectance infrared Fourier transform (DRIFT), the Pt-WO_x-MOF-74(Co) facilitated the conversion of glucose into intermediate and final products, which was dynamically detected. In conclusion, a certain synergy exists between Pt NPs, WO_x and MOF-74(Co), contributing to the high yield of 1,2-PDO. This work reports for the first time that MOFs can be used to convert glucose to lower diols in aqueous systems without structural damage and can be recycled many times. It breaks the spell that the structure of MOF materials will collapse in an aqueous solution environment with higher temperatures.

EXPERIMENTAL

Catalyst preparation

Synthesis of MOF-74(Co)

MOF-74(Co) was synthesized according to the previous work[28]. First, 273 mg of $Co(NO_3)_2 \cdot 6H_2O$ and 104 mg of 2,5-dihydroxyterephthalic acid were dissolved in a mixed solution of N,N-dimethylformamide (DMF, 20 mL) and deionized water (1 mL), sonicated to dissolve the solid, and reacted at 100 °C for 24 h. After cooling down to ambient temperature, the solid obtained was washed three times with DMF and methanol, respectively. Finally, it was allowed to dry at 60 °C overnight to obtain MOF-74(Co).

Synthesis of WO_x and Pt-WO_x

WO_x was synthesized according to the previously reported method[29]. A solution was prepared by dissolving 600 mg of WCl_6 in anhydrous ethanol (25 mL), which yielded a yellow solution. This solution was subsequently poured into a 50 mL Teflon-coated autoclave, which was then subjected to heating at a temperature of 160 °C for a period of 24 h. Once the heating process was complete, the autoclave was allowed to cool down to ambient temperature. The blue-colored WO_x precipitate, which had formed on the interior lining, was isolated by means of centrifugation. The precipitate was subsequently rinsed with deionized water and then dried under vacuum conditions in an oven set at 80 °C for the duration of one night. Pt-WO_x was synthesized in a similar way as WO_x, except that $Na_2PtCl_6 \cdot 6H_2O$ was added to the precursor. The actual Pt content in Pt-WO_x was 1.2 wt% measured by inductively coupled plasma optical emission spectroscopy (ICP-OES).

Synthesis of WO_x-MOF-74(Co)

A mixture consisting of 200 mg of MOF-74(Co) and 30 mg of WCl_6 was prepared by dissolving it in anhydrous ethanol (25 mL). This mixture was then poured into a 50 mL autoclave that was Teflon-lined, and the autoclave was heated to a temperature of 160 °C for 24 h. Following this, the autoclave was allowed to cool down to ambient temperature. The resulting solid product was subsequently washed with ethanol and then subjected to drying in a vacuum oven at a temperature of 80 °C for an entire night.

Synthesis of Pt-MOF-74(Co)

A mixture consisting of 200 mg of MOF-74(Co) and 10 mg of $Na_2PtCl_6·6H_2O$ was prepared by dissolving it in anhydrous ethanol (25 mL). This mixture was then poured into the 50 mL autoclave that was Teflon-lined, and the autoclave was heated to a temperature of 160 °C for 24 h. Following this, the autoclave was allowed to cool down to ambient temperature. The resulting solid product was subsequently washed with ethanol and then subjected to drying in a vacuum oven at a temperature of 80 °C for an entire night. The actual Pt content in Pt-MOF-74(Co) was 1.2 wt%.

Synthesis of Pt-WO_x-MOF-74(Co) and Pt/WO_x-MOF-74(Co)

A mixture consisting of 200 mg of MOF-74(Co), 30 mg of WCl_6 and 10 mg of $Na_2PtCl_6·6H_2O$ was prepared by dissolving it in anhydrous ethanol (25 mL). This mixture was then poured into a 50 mL autoclave that was Teflon-lined, and the autoclave was heated to a temperature of 160 °C for 24 h. Following this, the autoclave was allowed to cool down to ambient temperature. The resulting solid product was subsequently washed with ethanol and then subjected to drying in a vacuum oven at a temperature of 80 °C for an entire night. The actual Pt content in Pt-WO_x-MOF-74(Co) was 1.4 wt%. The Pt/WO_x-MOF-74(Co) catalyst was prepared by impregnating WO_x-MOF-74(Co) with $Na_2PtCl_6·6H_2O$, followed by a reduction process using hydrogen gas at a temperature of 200 °C for 4 h, resulting in the formation of Pt/WO_x-MOF-74(Co). The actual Pt content in Pt/WO_x-MOF-74(Co) was 1.2 wt%.

Catalytic reaction

The glucose catalytic conversion experiment was carried out in a 25 mL homemade stainless autoclave, and the results were analyzed by high-performance liquid chromatography (HPLC). The glucose conversion and product yield were calculated using glucose conversion (%) = 100% × (carbon atoms in the converted glucose) / (carbon atoms in the initial glucose); yield of product (%) = 100% × (carbon atoms in the product) / (carbon atoms in the initial glucose). Some by-products (such as aldehydes, carboxylic acids, furan compounds, humins, *etc.*) were not individually quantified, and no gaseous product was generated confirmed by gas chromatography (GC) analysis. The specific operation steps and analytic method were shown in the Supplementary Materials.

RESULTS AND DISCUSSION

Characterization of the prepared catalysts

MOF-74(Co) was synthesized according to the previously reported methods[28,30] with slight modifications and then reacted with WCl_6 and $Na_2PtCl_6·6H_2O$ to obtain Pt-WO_x-MOF-74(Co) [Figure 1A]. The morphology of the synthesized product was described by transmission electron microscopy (TEM). As shown in Supplementary Figure 2A and B, MOF-74(Co) exhibited an irregular morphology, while WO_x presented a blooming flower-like structure. After modification with WO_x, WO_x-MOF-74(Co) still displayed irregular morphology [Supplementary Figure 2C]. Figure 1B reveals that the incorporation of Pt did not change the flower-like morphology of WO_x. Notably, Pt-MOF-74(Co) and Pt-WO_x-MOF-74(Co) surfaces exhibited distinct metal nanoparticles [Supplementary Figure 3], with particle size distribution plots showing an average nanoparticle size of approximately 2.1 nm [Figure 1C and D]. High-angle annular dark

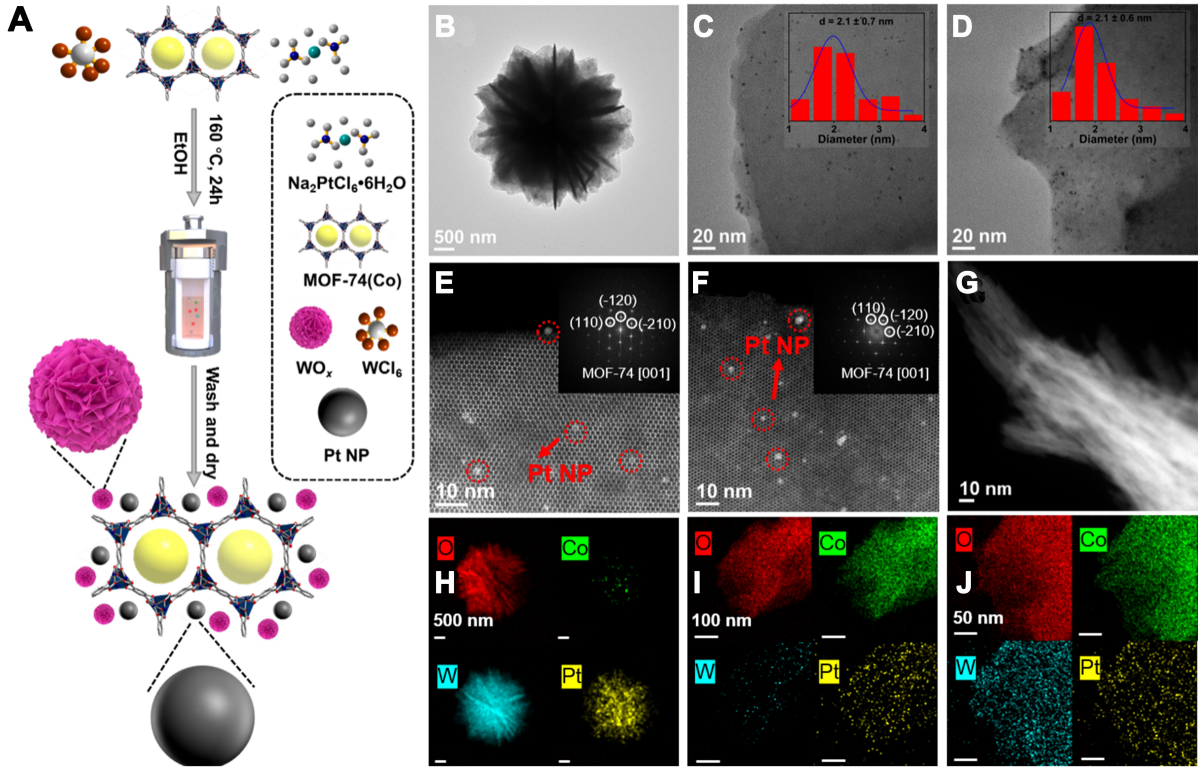

Figure 1. (A) Diagram of the preparation process of Pt-WO_x-MOF-74(Co); (B-D) TEM pictures of Pt-WO_x, Pt-MOF-74(Co) and Pt-WO_x-MOF-74(Co); (E and F) HAADF-STEM images from the [110] projection of Pt-MOF-74(Co) and Pt-WO_x-MOF-74(Co); (G) HAADF-STEM image of Pt-WO_x; (H-J) EDS elemental mappings of Pt-WO_x, Pt-MOF-74(Co) and Pt-WO_x-MOF-74(Co). MOF: Metal-organic framework; TEM: transmission electron microscopy; HAADF-STEM: high-angle annular dark field scanning TEM; EDS: energy-dispersive X-ray spectroscopy.

field scanning TEM (HAADF-STEM) images along the [001] crystal axis of Pt-MOF-74(Co) and Pt-WO_x-MOF-74(Co) are presented in Figure 1E and F. The MOF-74(Co) and WO_x-MOF-74(Co) frameworks remained crystalline post Pt loading, as confirmed by the Fourier transform in the inset images. The bright contrast features (examples marked with circles) in the HAADF-STEM images correspond to Pt NPs. These nanoparticles exhibited a relatively uniform size, larger than the pore size, indicating the presence of highly dispersed metal nanoparticles on the surface of Pt-MOF-74(Co) and Pt-WO_x-MOF-74(Co). The predominant fraction of the nanoparticles was crystallized Pt NPs, as evidenced by the HRTEM images [Supplementary Figure 4]. No obvious metal particles were observed in the HAADF-STEM image of Pt-WO_x [Figure 1G], while energy-dispersive X-ray spectroscopy (EDS) elemental mapping [Figure 1H] showed uniform Pt signals, probably because the WO_x layer was too thick and the Pt particles were too small, making it difficult to observe the Pt particles. The measured lattice spacing of Pt-MOF-74(Co) and Pt-WO_x-MOF-74(Co) was 0.22 nm, consistent with the lattice spacing of Pt(111)[31-33]. EDS elemental mappings [Figure 1I and J] showed that Pt was uniformly distributed on Pt-MOF-74(Co) and Pt-WO_x-MOF-74(Co), corroborating the HRTEM findings that the metal nanoparticles were indeed Pt. Supplementary Figure 5A showed the presence of metal clusters on WO_x-MOF-74(Co), and the EDS elemental mapping [Supplementary Figure 5B] revealed that W was uniformly distributed on WO_x-MOF-74(Co), suggesting that the metal clusters could be WO_x.

The crystal structure of the catalysts was determined by X-ray powder diffractometry (XRD). As displayed in Figure 2A and Supplementary Figure 6A, the positions of the first two peaks of WO_x-MOF-74(Co), Pt-

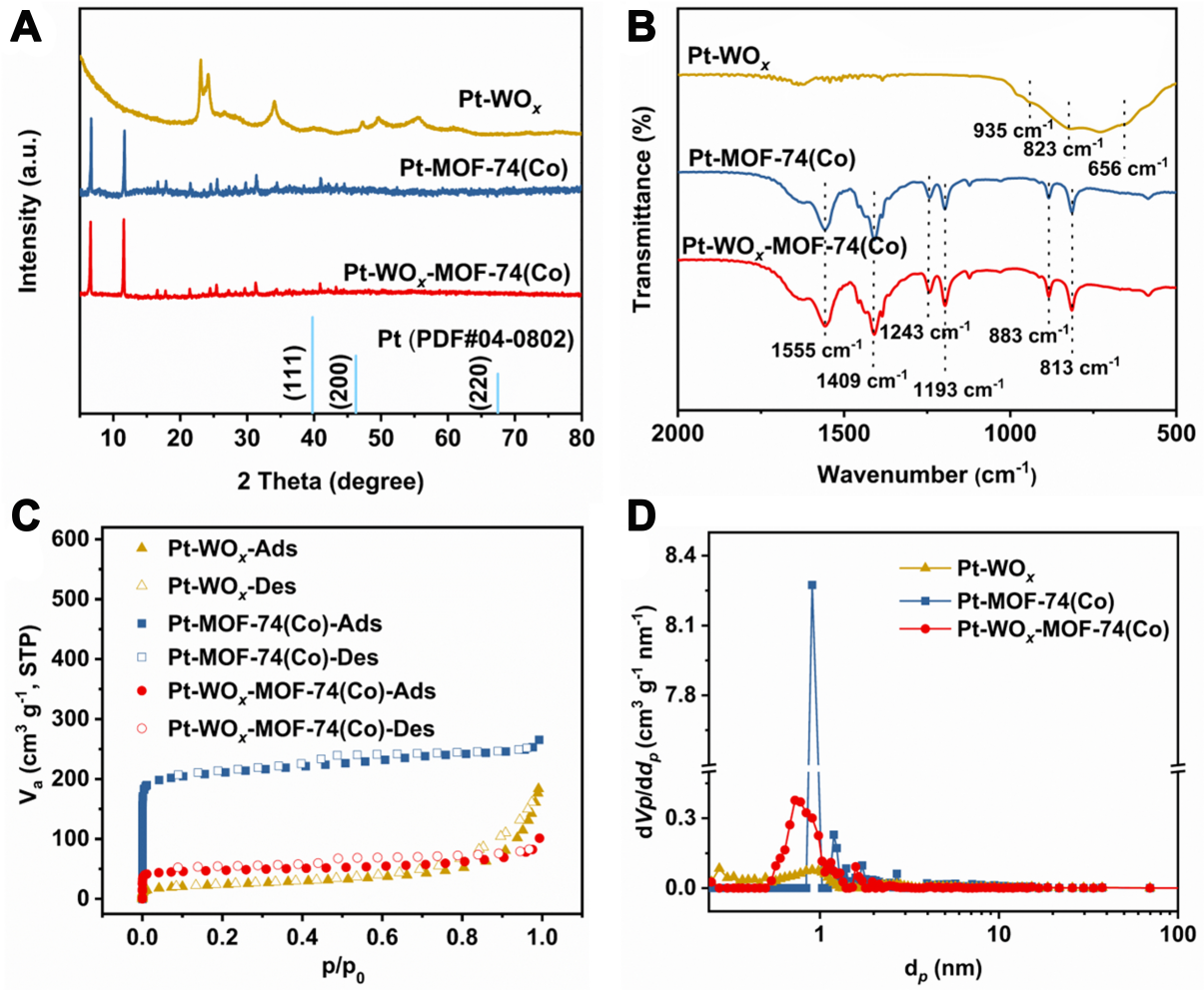

Figure 2. (A) XRD patterns, (B) FTIR spectra, (C) N_2 adsorption-desorption isotherms and (D) pore size distribution plots of the synthesized samples. XRD: X-ray powder diffractometry; FTIR: Fourier transform infrared.

MOF-74(Co), and Pt-WO_x-MOF-74(Co) matched well with the MOF-74(Co), indicating the Pt NPs and WO_x did not disrupt the crystal structure of MOF-74(Co). As a comparison, the XRD patterns of WO_x and Pt-WO_x were also measured and the results were identical to the literature[29]. There were no diffraction peaks belonging to WO_x and Pt NPs (PDF#04-0802) in Pt-WO_x-MOF-74(Co), probably due to the low content [Supplementary Table 1] and high dispersion of WO_x and Pt NPs. Thus, it was illustrated by XRD, ICP and TEM that Pt NPs were highly distributed on the MOF-74(Co) surface.

In addition, the Fourier transform infrared (FTIR) spectroscopy of the samples was performed [Figure 2B and Supplementary Figure 6B] to further validate the composition of the catalysts. The peaks were assigned as follows: 1,555 cm^{-1} represented the stretching vibration of C=O; 1,409 cm^{-1} represented the framework vibration of benzene ring; 1,243 and 1,193 cm^{-1} represented the stretching vibration of C–O; 883 and 813 cm^{-1} correspond to the out-of-plane bending vibration of C–H on the benzene ring; 697 cm^{-1} corresponded to the out-of-plane bending vibration of O–H[34]; 935 cm^{-1} represented the stretching vibration of W=O; 823 cm^{-1} represented the bending vibration of W-O-W; 656 cm^{-1} represented the stretching vibration of O–W–O[29]. The FTIR spectra of 2,5-dihydroxyterephthalic acid and MOF-74(Co) showed significant differences due to the deprotonation reaction of 2,5-dihydroxyterephthalic acid during the

formation of the MOF-74(Co) structure. Compared with MOF-74(Co), the FTIR spectra of WO_x-MOF-74(Co), Pt-MOF-74(Co), and Pt-WO_x-MOF-74(Co) did not show significant differences, suggesting the similar environment for 2,5-dioxido-1,4-benzenedicarboxylate ($DOBDC^{4-}$) in these materials. Moreover, the absence of characteristic bonds about WO_x in Pt-WO_x-MOF-74(Co) further indicated the low dose of WO_x.

The N_2 adsorption/desorption isotherms of the catalyst were shown in Figure 2C and Supplementary Figure 6C. Depending on the International Union of Pure and Applied Chemistry (IUPAC) classification of isotherm profiles[35], the isotherms of MOF-74(Co), WO_x-MOF-74(Co), Pt-MOF-74(Co), and Pt-WO_x-MOF-74(Co) were of type I, showing their microporous structures. MOF-74(Co), WO_x-MOF-74(Co), Pt-MOF-74(Co), and Pt-WO_x-MOF-74(Co) had large specific surface areas of 818, 699, 790, and 180 $m^2 \cdot g^{-1}$, respectively, which favored their catalytic activities. The decreased specific surface area of Pt-WO_x-MOF-74(Co) compared to MOF-74(Co) may be related to the occupation of MOF pores by Pt NPs and WO_x, which could also be seen from their pore volumes [Figure 2D, Supplementary Figure 6D and Supplementary Table 1], which were 0.7 and 0.2 $cm^3 \cdot g^{-1}$ for MOF-74(Co) and Pt-WO_x-MOF-74(Co), respectively.

The transformation of glucose into diols catalyzed by the synthesized catalysts

In aqueous-based reaction solutions, the reaction activity and product yields are significantly affected by the reaction parameters, including temperature and time. Consequently, an in-depth analysis was conducted to examine the impact of various reaction parameters, such as temperature, time, and catalyst dosage, on both the conversion of glucose and the yield of 1,2-PDO. The temperature dependence of glucose conversion was shown in Figure 3A. At a temperature of 140 °C, the conversion of glucose and the yield of 1,2-PDO were found to be 68.1% and 27.2%, respectively, which indicated a lower hydrogenolysis rate. When the reaction temperature was increased from 140 to 160 °C, the conversion increased to 100% and the yield of 1,2-PDO increased to 52.9%, the phenomenon suggesting that high temperature was an important factor in facilitating the reaction. However, a sustained increased in temperature to 180 °C resulted in a decreased in 1,2-PDO yield to 45.6%, which may be because high temperature promoted the dehydration reaction, resulting in cyclization and partial polycondensation of 1,2-PDO; thus, the production of 1,2-PDO was reduced. As displayed in Figure 3B, the reaction time was also an important factor affecting the conversion and product yield. For reaction durations shorter than 4 h, the glucose conversion did not exceed 80%, and the yield of 1,2-PDO remained below 25%. Extending the reaction time to 4 h, both the conversion and 1,2-PDO yield peaked at 100% and 52.9%, respectively. Prolonged reaction durations led to a reduction in the yield of 1,2-PDO. Consequently, a reaction duration of 4 h was identified as the most effective for maximizing 1,2-PDO production. As depicted in Figure 3C, the catalyst dosage significantly influences the yield of 1,2-PDO. Experimental results indicated that when the catalyst dosage is increased to 25 mg, the yield of 1,2-PDO reaches 33.4%. Further increasing the catalyst dosage to 100 mg elevated the 1,2-PDO yield to 45.6%. However, compared with the 52.6% yield of 1,2-PDO obtained with 50 mg of catalyst, additional increments in catalyst amount did not further enhance the yield. Consequently, it can be concluded that an optimal amount of catalyst is sufficient to effectively facilitate the conversion of glucose to 1,2-PDO, and excess catalyst does not contribute to increased yields. These findings provide empirical evidence for optimizing catalyst usage, contributing to the economic and efficient nature of the catalytic process.

In order to interpret more rigorously the effect of Pt-WO_x-MOF-74(Co) on glucose hydrogenolysis, the catalytic performance of Pt-WO_x-MOF-74(Co) was tested and compared with other catalysts [Figure 3D]. When no catalyst was present, glucose conversion was as low as 62.7% and 1,2-PDO was almost absent from the liquid phase product. When MOF-74(Co) or WO_x was used as a catalyst, glucose conversion was increased to 87.2% and 99.8%, respectively, but 1,2-PDO yields were lower than 10% for both. WO_x-MOF-74(Co) increased the yield of 1,2-PDO to 11.4%, indicating that WO_x favored the generation of 1,2-PDO.

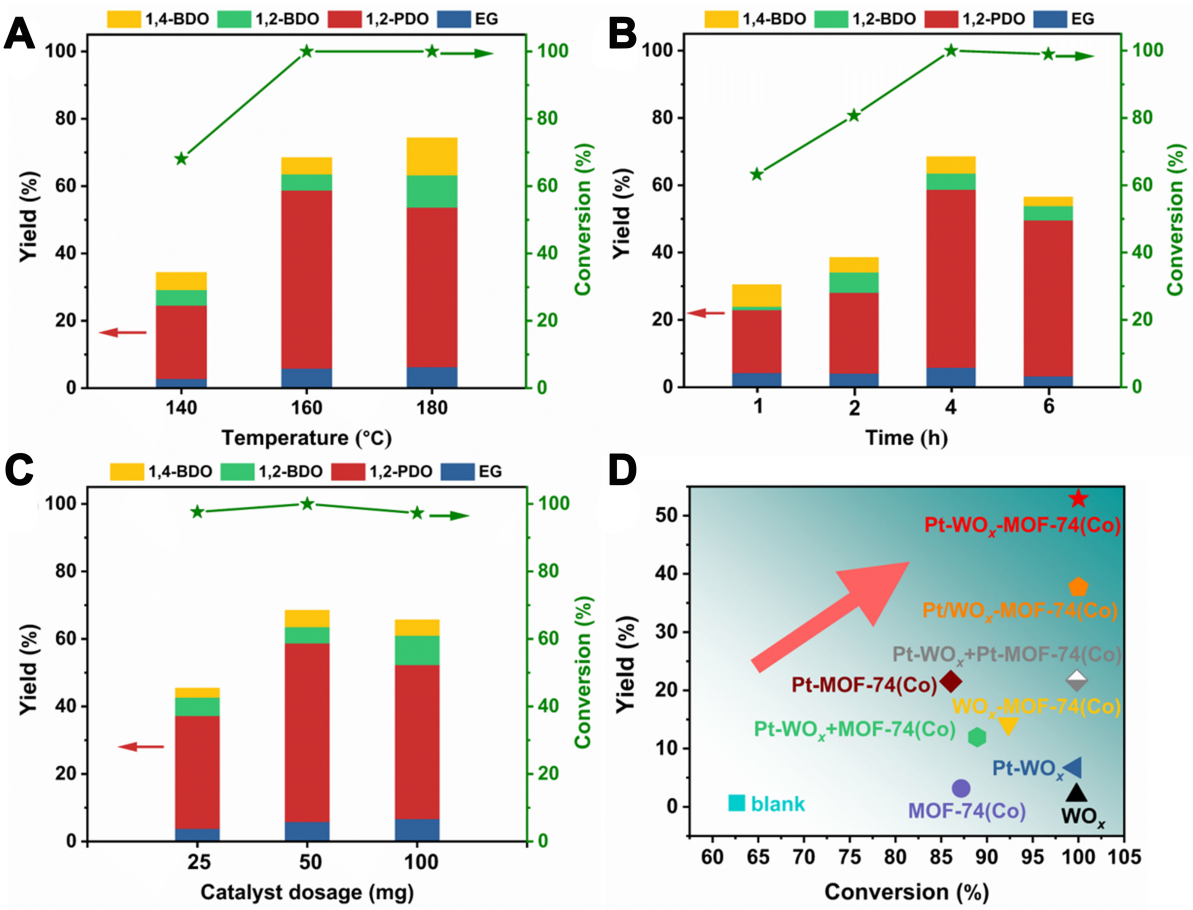

Figure 3. The influence of various reaction parameters on the conversion of glucose and the yield of diols using the Pt-WO_x-MOF-74(Co), (A) temperature, (B) reaction time, and (C) Pt-WO_x-MOF-74(Co) dosage; (D) The catalytic conversion of glucose to 1,2-PDO across a range of catalysts. Reaction conditions: glucose (100 mg), catalyst (50 mg) and water (10 mL), conducted at 160 °C, 0.2 MPa of H_2, for a period of 4 h. MOF: Metal-organic framework; 1,2-PDO: 1,2-propanediol.

Considering the effect of the carriers, the activities of Pt-MOF-74(Co) and Pt-WO_x were compared, and their conversions were 86.1% and 99.6%, while the 1,2-PDO yields were 21.5% and 6.7%, respectively, suggesting that MOF-74(Co) was the main reason to the great selectivity of 1,2-PDO. We physically mixed the samples [Pt-WO_x mixed with MOF-74(Co) or Pt-MOF-74(Co)] and found that mixing Pt-WO_x with Pt-MOF-74(Co) improved the conversion and 1,2-PDO yield to 99.8% and 21.7%, respectively. Under identical reaction parameters, the Pt-WO_x-MOF-74(Co) achieved a 1,2-PDO yield of up to 52.9%, surpassing numerous outcomes documented in the existing literature, as detailed in Supplementary Table 2. Wang *et al.* reported a 2%Pt/7.5%WO_x/Nano-Al_2O_3 catalyst that achieved a high yield of 1,2-PDO at 55.8% under relatively harsh reaction conditions (245 °C, 5 MPa H_2)[36]. In contrast, the Pt-WO_x-MOF-74(Co) catalyst used in our study realized a 1,2-PDO yield of 52.9% under much milder conditions (160 °C, 0.2 MPa H_2). Although both catalysts contain the same active components (Pt and W), the difference in support materials highlights the crucial role of the MOF-74(Co) support in facilitating the mild conversion of glucose to 1,2-PDO.

The 1,2-PDO yield of Pt/WO_x-MOF-74(Co) synthesized by the impregnation method was 37.7%, which was much lower than that of Pt-WO_x-MOF-74(Co). On the one hand, the specific surface area of Pt/WO_x-MOF-74(Co) was known to be 90 $m^2 \cdot g^{-1}$ through Supplementary Table 1, indicating that the active site of Pt/WO_x-

MOF-74(Co) was lower than that of Pt-WO_x-MOF-74(Co). XRD [Supplementary Figure 7A] tests showed that Pt/WO_x-MOF-74(Co) presented a similar structure to that of Pt-WO_x-MOF-74(Co). A TEM image [Supplementary Figure 7B] revealed significant aggregation of Pt NPs on Pt/WO_x-MOF-74(Co). The above-mentioned set of reasons led to the fact that Pt/WO_x-MOF-74(Co) was not as active as Pt-WO_x-MOF-74(Co). When we replaced glucose with the intermediate (1,3-dihydroxyacetone) [Supplementary Figure 8], we found that Pt-WO_x, Pt-MOF-74(Co) and Pt-WO_x-MOF-74(Co) could not convert 1,3-dihydroxyacetone completely and the yield of 1,2-PDO was lower than 50%. So, we guessed that the conversion of intermediates was not a decisive reason for the efficient conversion of glucose to 1,2-PDO by Pt-WO_x-MOF-74(Co).

We compared the glucose conversion, fructose yield and 1,2-PDO yield of Pt-WO_x, Pt-MOF-74(Co) and Pt-WO_x-MOF-74(Co) at 140 °C [Figure 4]. The glucose conversion of Pt-WO_x, Pt-MOF-74(Co) and Pt-WO_x-MOF-74(Co) showed an upward trend with increasing reaction time, suggesting that glucose was continuously converted to the target products (e.g., fructose and 1,2-PDO). When the reaction time was 2 h, we found that more fructose was produced when MOF-74(Co) was present, and as the time increased, the fructose decreased, implying that the fructose was further converted to some product (probably 1,2-PDO). For Pt-WO_x, the decrease of fructose did not promote the generation of 1,2-PDO [Figure 4A], whereas, for Pt-MOF-74(Co) and Pt-WO_x-MOF-74(Co) [Figure 4B and C], the increment in 1,2-PDO corresponded to a reduction in fructose, further confirming that 1,2-PDO was the primary conversion product derived from fructose. The 1,2-PDO yield of Pt-WO_x-MOF-74(Co) decreased when the reaction time was extended to 6 h, probably due to the long reaction time might lead to the competitive reaction of the by-products (including aldehydes, carboxylic acids, furan derivatives and humic acids) with 1,2-PDO; therefore, the 1,2-PDO yield decreased. Figure 4 demonstrated that MOF-74(Co) played a critical role in the conversion of glucose to 1,2-PDO; i.e., MOF-74(Co) promoted the conversion of glucose to fructose so that fructose could be rapidly converted to 1,2-PDO.

An in-depth study on the superior catalytic performance of Pt-WO_x-MOF-74(Co)

To reveal the reason for the excellent activity of Pt-WO_x-MOF-74(Co) at a deeper level, we next performed a series of characterization analyses. XPS was utilized to analyze the surface components and chemical states of the catalysts. Figure 5A showed the W 4f XPS spectrum of Pt-WO_x and Pt-WO_x-MOF-74(Co); the peaks located at 35.5 and 37.7 eV could be attributed to W $4f_{7/2}$ and W $4f_{5/2}$ of the W^{5+} species, whereas the other double peaks located at 36.1 and 38.3 eV could be attributed to W $4f_{7/2}$ and W $4f_{5/2}$ of the W^{6+} species, respectively[37]. The W^{5+}/W^{6+} of Pt-WO_x and Pt-WO_x-MOF-74(Co) were 0.4 and 0.6 [Supplementary Table 3], respectively, suggesting that more W^{6+} species in Pt-WO_x-MOF-74(Co) were reduced to W^{5+} species, subsequently creating a higher concentration of oxygen vacancies[38-40]. Oxygen vacancies could be used as Lewis acid sites[41,42], suggesting that Pt-WO_x-MOF-74(Co) had higher acid content.

In the analysis of XPS, the O1s peak of the Pt-WO_x catalyst [Supplementary Figure 9] could be resolved into a triplet structure. These peaks were attributed to lattice oxygen (O_{lat}), hydroxyl oxygen (O–H), and adsorbed oxygen atoms on the surface (O_{ads})[43,49]. Similarly, the O1s XPS peak of the Pt-WO_x-MOF-74 (Co) catalyst [Supplementary Figure 9] also exhibited a triplet feature, corresponding to C=O, O–H, and Co–O bonds[43-45,50]. The existence of oxygen vacancies was confirmed by EPR, as illustrated in Figure 5B. The EPR signal observed at g = 2.002 is indicative of electrons being trapped within oxygen vacancy sites[51-53]; it is reasonable to infer that Pt-WO_x-MOF-74(Co) had significant oxygen vacancies.

Considering that suitable acid sites played a key role in facilitating the biomass conversion process, the acid sites of the catalyst were detected using pyridine-adsorbed DRIFT spectroscopy (DRIFTS) [Figure 6A-C].

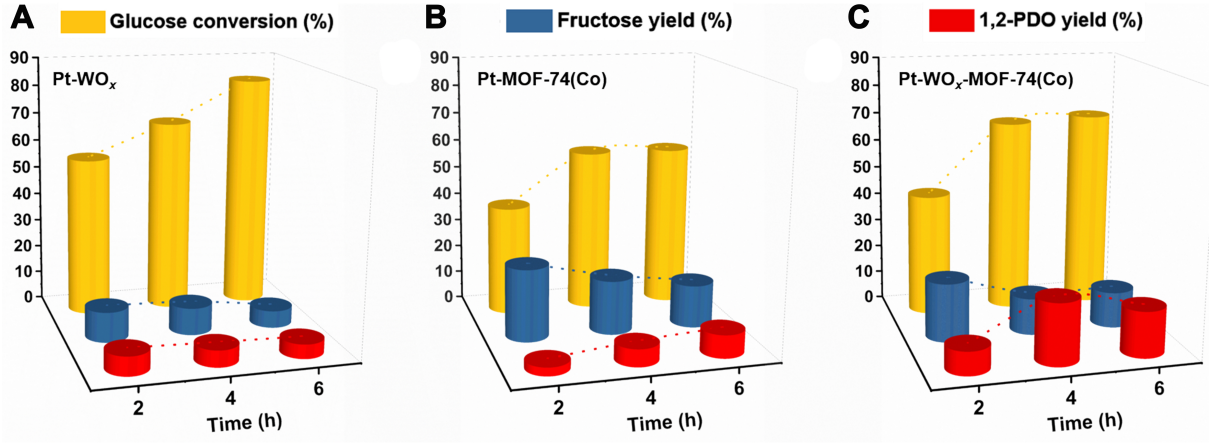

Figure 4. The glucose conversion, fructose yield and 1,2-PDO yield of Pt-WO_x, Pt-MOF-74(Co) and Pt-WO_x-MOF-74(Co). Reaction conditions: glucose (100 mg), catalyst (50 mg) and water (10 mL), 140 °C, 0.2 Mpa of H_2. 1,2-PDO: 1,2-Propanediol; MOF: metal-organic framework.

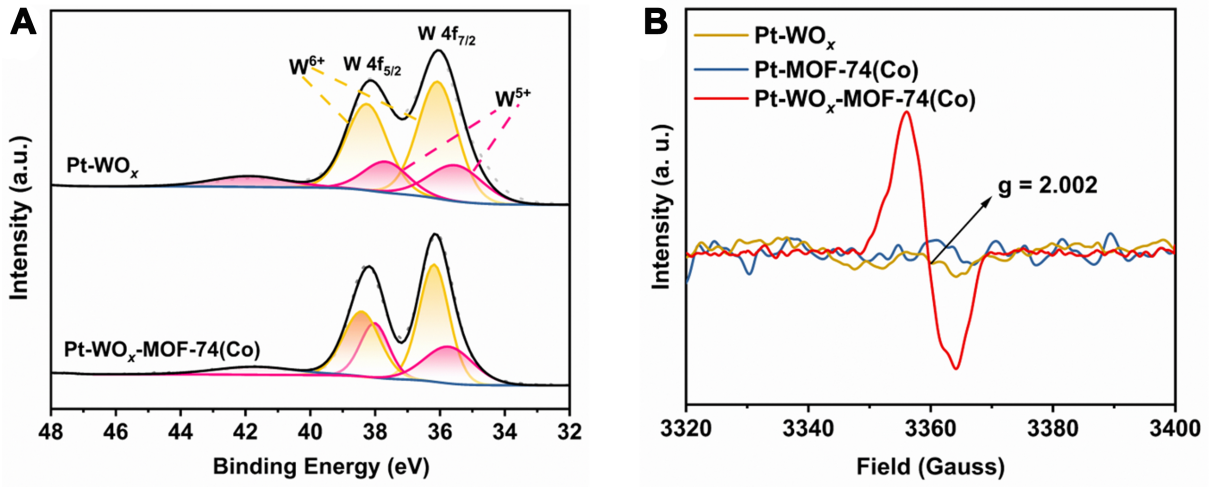

Figure 5. (A) W 4f XPS, (B) EPR of these three catalysts. XPS: X-ray photoelectron spectroscopy; EPR: electron paramagnetic resonance.

The absorption bands at 1,451 and 1,600 cm^{-1} in the spectrum were assigned to Lewis acid sites, whereas the bands at 1,538 and 1,664 cm^{-1} were indicative of Brönsted acid sites. Additionally, the band observed at 1,488 cm^{-1} represented a combined feature of both Lewis and Brönsted acid sites[54,55]. Pyridine desorption was noted to occur from Pt-WO_x at a temperature of 300 °C. In contrast, the pyridine molecules adsorbed onto both Pt-MOF-74(Co) and Pt-WO_x-MOF-74(Co) exhibited negligible desorption at the same temperature, maintaining their stability. The aforementioned results revealed that MOF-74(Co) was favorable to maintaining the acid strength stable, but the better activity of Pt-WO_x-MOF-74(Co) compared with Pt-MOF-74(Co) deserved to be further explored.

The intensity and total acid amount of the acidic sites of Pt-MOF-74(Co) and Pt-WO_x-MOF-74(Co) were determined using NH_3-TPD curves. Figure 6D illustrated that the Pt-MOF-74(Co) and Pt-WO_x-MOF-74(Co) exhibited two significant peaks within the temperature region of approximately 500 °C, indicative of the presence of strong acid sites within their structures. The total acid amount was 5.9 mmol·g^{-1} in Pt-WO_x-MOF-74(Co) and 3.3 mmol·g^{-1} in Pt-MOF-74(Co) [Supplementary Table 1], suggesting that the

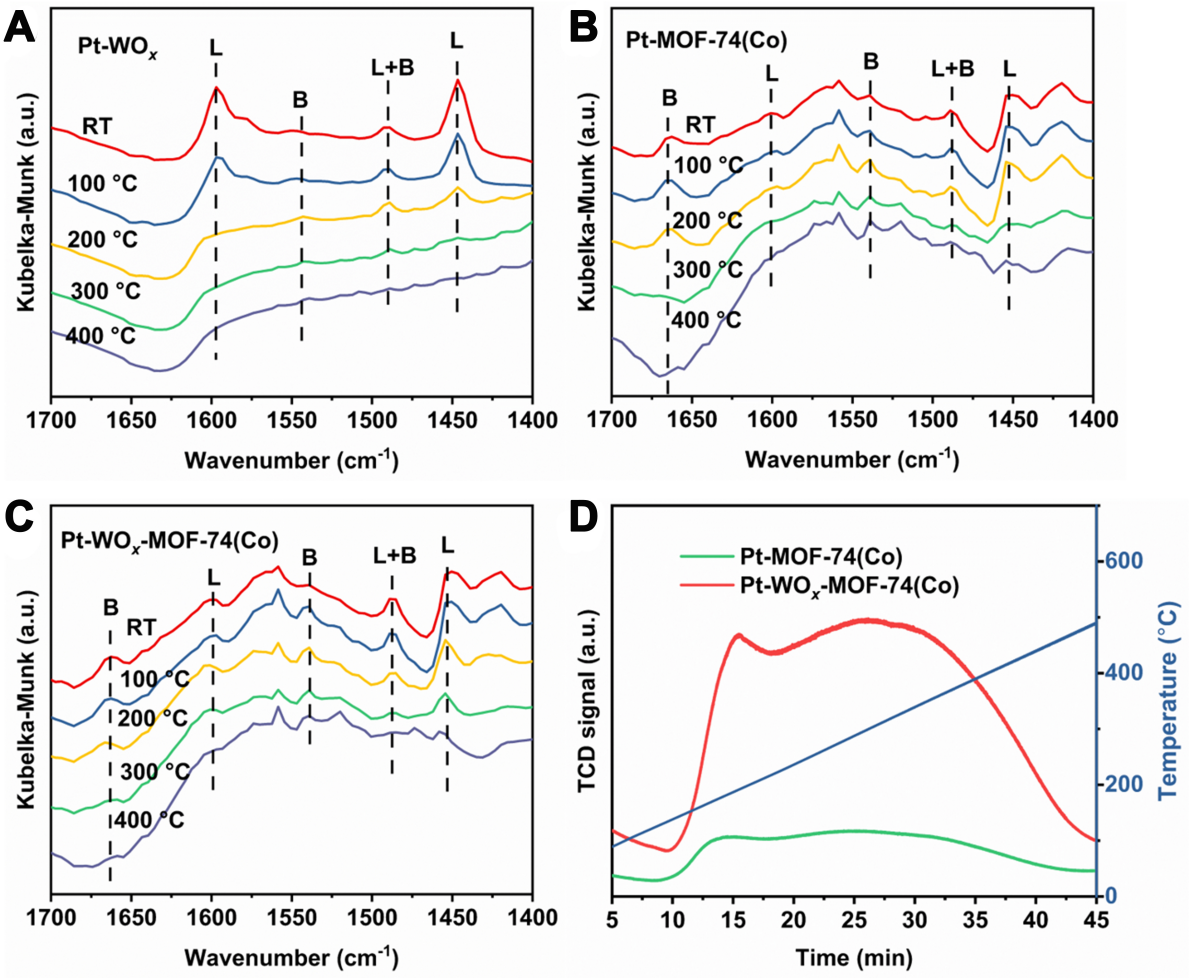

Figure 6. Pyridine-adsorbed DRIFTS spectra of (A) Pt-WO$_x$, (B) Pt-MOF-74(Co) and (C) Pt-WO$_x$-MOF-74(Co); (D) NH_3-TPD-MS curve of Pt-MOF-74(Co) and Pt-WO$_x$-MOF-74(Co). DRIFTS: Diffuse reflectance infrared Fourier transform spectroscopy; MOF: metal-organic framework; NH_3-TPD: NH_3 temperature-programmed desorption.

incorporation of WO$_x$ into the Pt-WO$_x$-MOF-74(Co) enhanced the creation of acidic sites, which was consistent with the EPR.

Further investigation of the conversion of glucose to 1,2-PDO by *in situ* DRIFTS

The *in situ* DRIFTS spectra of chemoselective transformation process of glucose were shown in Figure 7. Single Pt-WO$_x$-MOF-74(Co) and glucose-impregnated Pt-WO$_x$-MOF-74(Co) [Pt-WO$_x$-MOF-74(Co)-G] were kept at room temperature for 30 min (black line). As the temperature increased, a series of distinct bands appeared in Pt-WO$_x$-MOF-74(Co), in which the bands near 1,000-1,500 cm^{-1} and at 1,608 cm^{-1} were from the C–O and C=O bonds of the catalyst, respectively[56,57]. The bands of Pt-WO$_x$-MOF-74(Co)-G located around 1,000-1,500 cm^{-1} were different from those of Pt-WO$_x$-MOF-74(Co), suggesting that these were C–O belonging to glucose, and as the temperature increased, the bands around 1,000-1,150 cm^{-1} receded significantly due to the glycosidic bonds and pyran rings cleavaged into volatiles[57]. Furthermore, the carbonyl group (C=O) absorption band at 1,777 cm^{-1}[56] began to manifest around 100 °C, with its intensity escalating as the temperature rose, peaking at approximately 200 °C. The increase in the C=O signal corresponds to the primary phase of glucose conversion[58], indicating that the C–O and C–C bonds in the glucose molecule were cleaved to form intermediates[57,59]. The aforementioned findings confirm the

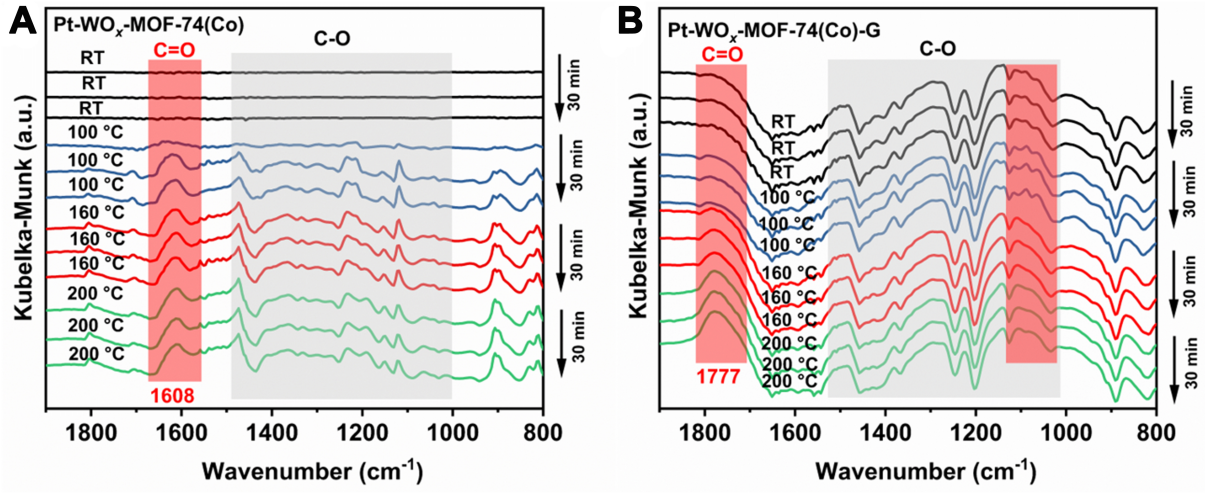

Figure 7. DRIFTS spectroscopy of (A) single Pt-WO_x-MOF-74(Co) and (B) glucose-impregnated Pt-WO_x-MOF-74(Co) at varying temperatures. DRIFTS: Diffuse reflectance infrared Fourier transform spectroscopy; MOF: metal-organic framework.

effective transformation of glucose into intermediate compounds facilitated by the Pt-WO_x-MOF-74(Co) catalyst, subsequently leading to the production of 1,2-PDO.

Stability experiments of Pt-WO_x-MOF-74(Co) and the generalization in raw biomass conversion

The recycling experiment of Pt-WO_x-MOF-74(Co) was shown in Supplementary Figure 10A. The catalyst, after the reaction, was recovered by centrifugation, rinsed extensively with ethanol, and then vacuum-dried overnight in an oven before proceeding to the next reaction cycle. It can be seen that such catalyst activity decreased slightly during six consecutive cycles. XRD pattern of the recycled catalyst [Supplementary Figure 10B] maintained its crystallinity during the recycling tests. Although thermal filtration tests showed that the yield of 1,2-PDO maintained around 20% after removing Pt-WO_x-MOF-74(Co) from the reaction mixture [Supplementary Figure 10C], leaching of a little part of active Pt and W- species and slight agglomeration of Pt NPs occurred [Supplementary Table 1 and Supplementary Figure 10D], which were not the key factors to result in the reduction of catalytic activity. From Supplementary Table 1, the Brunauer–Emmett–Teller (BET) specific surface area of the recovered catalyst greatly decreased to 52 $m^2 \cdot g^{-1}$, which meant that some unknown impurities covered the surface of such catalyst during the recycling process. After treatment by H_2O_2 to eliminate these carbonaceous species, the yield of 1,2-PDO can be recovered, demonstrating that Pt-WO_x-MOF-74(Co) could be reused stably under optimal reaction conditions.

In order to investigate the generalization of Pt-WO_x-MOF-74(Co) in the reaction of raw biomass conversion for the preparation of diols, several different biomasses were selected as reactants. As shown in Supplementary Table 4, Pt-WO_x-MOF-74(Co) could rapidly prepare 1,2-PDO from corncob, xylan, and starch, whose yields were 26.5%, 30.4%, and 27.9%, respectively, confirming the generalizability of Pt-WO_x-MOF-74(Co) in the preparation of 1,2-PDO-derived biomass. However, the yield of 1,2-PDO derived from these substrates was much lower than that from glucose, which was mainly due to the difficulty of hydrolysis of these substrates to active mono-carbohydrates over Pt-WO_x-MOF-74(Co) catalyst. Future work to improve 1,2-PDO yield from raw biomass is still ongoing.

CONCLUSIONS

The synergistic interaction of Pt NPs, WO_x and MOF-74(Co) was realized by a facile and efficient two-step method. The synthesized Pt-WO_x-MOF-74(Co) demonstrated superior catalytic activity for the conversion

of biomass into 1,2-PDO. When glucose was used as the substrate, the yield of 1,2-PDO was as high as 52.9% under milder reaction conditions (160 °C, 0.2 MPa H_2, 4 h), which outperformed most of other reported catalysts. Moreover, the catalyst was able to be reused several times. The reason for the efficient catalytic activity of Pt-WO_x-MOF-74(Co) was explained in detail by various characterization results including XPS, EPR, NH_3-TPD, *etc.* This work contributed to the design of efficient MOF catalysts for the production of high-value-added chemicals from biomass.

DECLARATIONS

Authors' contributions

Manuscript design, preparation, and revision: Luo, S.; Wang, J.
Manuscript discussion and preparation: Luo, S.; Mao, M.; Yu, H.; Zheng, Y.; Liu, Z.; Liu, L.; Wang, J.

Availability of data and materials

The detailed materials and methods in the experiment were listed in the Supplementary Materials. Other raw data that support the findings of this study are available from the corresponding author upon reasonable request.

Financial support and sponsorship

Wang, J. is grateful for the financial support from Chongqing Human Resources and Social Security Bureau Project (cx2024049), State Key Laboratory of Coal Mine Disaster Dynamics and Control (2011DA105287-MS202203), Natural Science Foundation of Chongqing (CSTB2022NSCQ-MSX0458), and Joint Fund for Innovation and Development of Chongqing (CSTB2022NSCQ-LZX0030). Liu, L. acknowledges the financial support from the National Natural Science Foundation of China (22105028) and the Natural Science Foundation of Chongqing (cstc2021jcyj-msxmX0572). Liu, Z. appreciates the financial support from the National Natural Science Foundation of China (22102013). This research used resources from the Analytical and Testing Center of Chongqing University.

Conflicts of interest

All authors declared that there are no conflicts of interest.

Ethical approval and consent to participate

Not applicable.

Consent for publication

Not applicable.

REFERENCES

1. Jiang, H.; Wu, X.; Zhang, H.; et al. Toward effective electrocatalytic C–N coupling for the synthesis of organic nitrogenous compounds using CO_2 and biomass as carbon sources. *SusMat* **2023**, *3*, 781-820. DOI
2. Wu, X.; Yan, Q.; Wang, H.; et al. Heterostructured catalytic materials as advanced electrocatalysts: classification, synthesis, characterization, and application. *Adv. Funct. Mater.* **2024**, *34*, 2404535. DOI
3. Zhang, Z.; Song, J.; Han, B. Catalytic transformation of lignocellulose into chemicals and fuel products in ionic liquids. *Chem. Rev.* **2017**, *117*, 6834-80. DOI
4. Sudarsanam, P.; Zhong, R.; Van den Bosch, S.; Coman, S. M.; Parvulescu, V. I.; Sels, B. F. Functionalised heterogeneous catalysts for sustainable biomass valorisation. *Chem. Soc. Rev.* **2018**, *47*, 8349-402. DOI PubMed
5. Mane, R.; Jeon, Y.; Rode, C. A review on non-noble metal catalysts for glycerol hydrodeoxygenation to 1,2-propanediol with and without external hydrogen. *Green. Chem.* **2022**, *24*, 6751-81. DOI

6. Zhao, H.; Zheng, L.; Li, X.; Chen, P.; Hou, Z. Hydrogenolysis of glycerol to 1,2-propanediol over Cu-based catalysts: a short review. *Catal. Today.* **2020**, *355*, 84-95. DOI
7. Główka, M.; Krawczyk, T. New trends and perspectives in production of 1,2-propanediol. *ACS. Sustain. Chem. Eng.* **2023**, *11*, 7274-87. DOI
8. Zheng, M.; Pang, J.; Sun, R.; Wang, A.; Zhang, T. Selectivity control for cellulose to diols: dancing on eggs. *ACS. Catal.* **2017**, *7*, 1939-54. DOI
9. Gu, M.; Shen, Z.; Yang, L.; et al. Reaction route selection for cellulose hydrogenolysis into C_2/C_3 glycols by ZnO-modified Ni-W/β-zeolite catalysts. *Sci. Rep.* **2019**, *9*, 11938. DOI PubMed PMC
10. Pang, J.; Zheng, M.; Li, X.; et al. Selective conversion of concentrated glucose to 1,2-propylene glycol and ethylene glycol by using RuSn/AC catalysts. *Appl. Catal. B. Environ.* **2018**, *239*, 300-8. DOI
11. Yazdani, P.; Wang, B.; Du, Y.; Kawi, S.; Borgna, A. Lanthanum oxycarbonate modified Cu/Al_2O_3 catalysts for selective hydrogenolysis of glucose to propylene glycol: base site requirements. *Catal. Sci. Technol.* **2017**, *7*, 4680-90. DOI
12. Kirali AA, Sreekantan S, Marimuthu B. Ce promoted Cu/γ-Al_2O_3 catalysts for the enhanced selectivity of 1,2-propanediol from catalytic hydrogenolysis of glucose. *Catal. Commun.* **2022**, *165*, 106447. DOI
13. Baniamerian, H.; Høj, M.; Beier, M. J.; Jensen, A. D. Catalytic conversion of sugars and polysaccharides to glycols: a review. *Appl. Catal. B. Environ.* **2023**, *330*, 122650. DOI
14. Yang, Y.; Ren, D.; Shang, C.; Ding, Z.; Luo, X. Site isolated Ru clusters and sulfoacids in a yolk-shell nanoreactor towards cellulose valorization to 1,2-propylene glycol. *Chem. Eng. J.* **2023**, *452*, 139206. DOI
15. Xin, Q.; Yu, S.; Jiang, L.; et al. Bifunctional catalyst with a Yolk–Shell structure catalyzes glucose to produce ethylene glycol. *J. Phys. Chem. C.* **2021**, *125*, 6632-42. DOI
16. Yazdani, P.; Wang, B.; Rimaz, S.; Kawi, S.; Borgna, A. Glucose hydrogenolysis over Cu-La_2O_3/Al_2O_3: mechanistic insights. *Mol. Catal.* **2019**, *466*, 138-45. DOI
17. Gu, M.; Shen, Z.; Zhang, W.; et al. Hydrogenolysis of glucose into propylene glycol over Pt/SiO_2@$Mg(OH)_2$ catalyst. *ChemCatChem* **2020**, *12*, 3447-52. DOI
18. Lv, M.; Zhang, Y.; Xin, Q.; et al. Pd@Al-containing mesoporous silica Yolk–Shell-structured nanospheres as high performance nanoreactors for the selective hydrogenolysis of glucose to 1,2-propylene glycol. *Chem. Eng. J.* **2020**, *396*, 125274. DOI
19. Liu, C.; Zhang, C.; Sun, S.; et al. Effect of WO_x on bifunctional Pd–WO_x/Al_2O_3 catalysts for the selective hydrogenolysis of glucose to 1,2-propanediol. *ACS. Catal.* **2015**, *5*, 4612-23. DOI
20. Ji, J.; Xu, Y.; Liu, Y.; Zhang, Y. A nanosheet Ru/WO_3 catalyst for efficient conversion of glucose to butanediol. *Catal. Commun.* **2020**, *144*, 106074. DOI
21. Liu, Y.; Liu, Y.; Zhang, Y. The synergistic effects of Ru and WO_x for aqueous-phase hydrogenation of glucose to lower diols. *Appl. Catal. B. Environ.* **2019**, *242*, 100-8. DOI
22. Luo, S.; Shu, T.; Mao, M.; et al. Efficient hydrogenolysis of fructose to 1,2-propanediol over bifunctional Ru-WO-MgO catalysts under mild reaction conditions via enhancing the chemoselective cleavage of C–C bonds. *J. Energy. Chem.* **2024**, *92*, 311-21. DOI
23. Lee, T. H.; Jung, J. G.; Kim, Y. J.; et al. Defect engineering in metal-organic frameworks towards advanced mixed matrix membranes for efficient propylene/propane separation. *Angew. Chem. Int. Ed. Engl.* **2021**, *60*, 13081-8. DOI
24. Cai, G.; Jiang, H. L. A modulator-induced defect-formation strategy to hierarchically porous metal-organic frameworks with high stability. *Angew. Chem. Int. Ed. Engl.* **2017**, *56*, 563-7. DOI PubMed
25. Jiao, L.; Seow, J. Y. R.; Skinner, W. S.; Wang, Z. U.; Jiang, H. Metal–organic frameworks: structures and functional applications. *Mater. Today.* **2019**, *27*, 43-68. DOI
26. Huang, G.; Yang, Q.; Xu, Q.; Yu, S.; Jiang, H. Polydimethylsiloxane coating for a palladium/MOF composite: highly improved catalytic performance by surface hydrophobization. *Angew. Chem. Int. Ed. Engl.* **2016**, *128*, 7505-9. DOI
27. Insyani, R.; Verma, D.; Cahyadi, H. S.; et al. One-pot di- and polysaccharides conversion to highly selective 2,5-dimethylfuran over Cu-Pd/Amino-functionalized Zr-based metal-organic framework (UiO-66(NH2))@SGO tandem catalyst. *Appl. Catal. B. Environ.* **2019**, *243*, 337-54. DOI
28. Heidary, N.; Chartrand, D.; Guiet, A.; Kornienko, N. Rational incorporation of defects within metal-organic frameworks generates highly active electrocatalytic sites. *Chem. Sci.* **2021**, *12*, 7324-33. DOI PubMed PMC
29. Li, Z.; Lu, X.; Sun, W.; et al. One-step synthesis of single palladium atoms in $WO_{2.72}$ with high efficiency in chemoselective hydrodeoxygenation of vanillin. *Appl. Catal. B. Environ.* **2021**, *298*, 120535. DOI
30. Wu, D.; Guo, Z.; Yin, X.; et al. Metal-organic frameworks as cathode materials for Li-O_2 batteries. *Adv. Mater.* **2014**, *26*, 3258-62. DOI
31. Yang, Q.; Gao, D.; Li, C.; et al. Highly dispersed Pt on partial deligandation of Ce-MOFs for furfural selective hydrogenation. *Appl. Catal. B. Environ.* **2023**, *328*, 122458. DOI
32. Wang, M.; Xu, Y.; Peng, C. K.; et al. Site-specified two-dimensional heterojunction of Pt nanoparticles/metal-organic frameworks for enhanced hydrogen evolution. *J. Am. Chem. Soc.* **2021**, *143*, 16512-8. DOI
33. Zahid, M.; Ismail, A.; Sohail, M.; Zhu, Y. Improving selective hydrogenation of carbonyls bond in α, β-unsaturated aldehydes over Pt nanoparticles encaged within the amines-functionalized MIL-101-NH_2. *J. Colloid. Interface. Sci.* **2022**, *628*, 141-52. DOI PubMed
34. Deng, X.; Yang, L.; Huang, H.; et al. Shape-defined hollow structural Co-MOF-74 and metal nanoparticles@Co-MOF-74 composite through a transformation strategy for enhanced photocatalysis performance. *Small* **2019**, *15*, e1902287. DOI
35. Sing, K. S. W.; Williams, R. T. Physisorption hysteresis loops and the characterization of nanoporous materials. *Adsorpt. Sci. Technol.*

2004, *22*, 773-82. https://www.researchgate.net/publication/42790927_Physisorption_Hysteresis_Loops_and_the_Characterization_of_Nanoporous_Materials. (accessed on 2025-03-14)

36. Wang, Z.; Li, W.; Zhang, Z.; Jia, L.; Wang, J. Effects of different Al_2O_3 supports on Pt/WO_x-based catalysts for selective hydrogenolysis of glucose to 1,2-propylene glycol. *ACS. Sustain. Chem. Eng.* **2023**, *11*, 17331-9. DOI
37. Feng, Y.; Wang, C.; Cui, P.; et al. Ultrahigh photocatalytic CO_2 reduction efficiency and selectivity manipulation by single-tungsten-atom oxide at the atomic step of TiO_2. *Adv. Mater.* **2022**, *34*, e2109074. DOI
38. Xiao, L.; Li, G.; Yang, Z.; et al. Engineering of amorphous PtO_x interface on Pt/WO_3 nanosheets for ethanol oxidation electrocatalysis. *Adv. Funct. Mater.* **2021**, *31*, 2100982. DOI
39. Cao, Y.; Wang, J.; Kang, M.; Zhu, Y. Catalytic conversion of glucose and cellobiose to ethylene glycol over Ni–WO_3/SBA-15 catalysts. *RSC. Adv.* **2015**, *5*, 90904-12. DOI
40. Hamdy, M. S.; Eissa, M. A.; Keshk, S. M. A. S. New catalyst with multiple active sites for selective hydrogenolysis of cellulose to ethylene glycol. *Green. Chem.* **2017**, *19*, 5144-51. DOI
41. Wang, F.; Ueda, W.; Xu, J. Detection and measurement of surface electron transfer on reduced molybdenum oxides (MoO_x) and catalytic activities of Au/MoO_x. *Angew. Chem. Int. Ed. Engl.* **2012**, *51*, 3883-7. DOI
42. Zhao, X.; Wang, J.; Yang, M.; et al. Selective hydrogenolysis of glycerol to 1,3-propanediol: manipulating the frustrated lewis pairs by introducing gold to Pt/WO*x*. *ChemSusChem* **2017**, *10*, 818. DOI
43. Idriss, H. On the wrong assignment of the XPS O1s signal at 531-532 eV attributed to oxygen vacancies in photo- and electro-catalysts for water splitting and other materials applications. *Surf. Sci.* **2021**, *712*, 121894. DOI
44. Morgan, D. J. Photoelectron spectroscopy of ceria: reduction, quantification and the myth of the vacancy peak in XPS analysis. *Surf. Interf. Anal.* **2023**, *55*, 845-50. DOI
45. Frankcombe, T. J.; Liu, Y. Interpretation of oxygen 1s X-ray photoelectron spectroscopy of ZnO. *Chem. Mater.* **2023**, *35*, 5468-74. DOI
46. Wang, B.; Wang, R.; Liu, L.; Wang, C.; Zhang, Y.; Sun, J. WO_3 nanosheet/$W_{18}O_{49}$ nanowire composites for NO_2 sensing. *ACS. Appl. Nano. Mater.* **2020**, *3*, 5473-80. DOI
47. Wang, Z.; Lin, R.; Huo, Y.; Li, H.; Wang, L. Formation, detection, and function of oxygen vacancy in metal oxides for solar energy conversion. *Adv. Funct. Mater.* **2022**, *32*, 2109503. DOI
48. Liu, J.; Ma, M.; Yu, X.; Xin, C.; Li, M.; Li, S. Constructing Ag decorated ZnS_{1-x} quantum dots/Ta_2O_{5-x} nanospheres for boosted tetracycline removal: synergetic effects of structural defects, S-scheme heterojunction, and plasmonic effects. *J. Colloid. Interf. Sci.* **2022**, *623*, 1085-100. DOI
49. Li, Y.; Wang, H.; Liu, Y.; et al. Bimetallic PtRu alloy nanocrystal-functionalized flower-like WO_3 for fast detection of xylene. *Sensor. Actuat. B. Chem.* **2022**, *351*, 130950. DOI
50. Pei, Y.; Ye, C.; Pei, X.; Li, W. Xylene adsorption behaviors of Co-MOF-74(X) synthesized from Co(II) salt with different anions. *Inorg. Chim. Acta.* **2024**, *568*, 122083. DOI
51. Yin, D.; Cao, Y.; Chai, D.; et al. A WO_x mediated interface boosts the activity and stability of Pt-catalyst for alkaline water splitting. *Chem. Eng. J.* **2022**, *431*, 133287. DOI
52. Ming, X.; Guo, A.; Wang, G.; Wang, X. Two-dimensional defective tungsten oxide nanosheets as high performance photo-absorbers for efficient solar steam generation. *Sol. Energy. Mater. Sol. Cells.* **2018**, *185*, 333-41. DOI
53. Bo, Y.; Wang, H.; Lin, Y.; et al. Altering hydrogenation pathways in photocatalytic nitrogen fixation by tuning local electronic structure of oxygen vacancy with dopant. *Angew. Chem. Int. Ed. Engl.* **2021**, *60*, 16085-92. DOI
54. Zholobenko, V.; Freitas, C.; Jendrlin, M.; Bazin, P.; Travert, A.; Thibault-Starzyk, F. Probing the acid sites of zeolites with pyridine: quantitative AGIR measurements of the molar absorption coefficients. *J. Catal.* **2020**, *385*, 52-60. DOI
55. Xu, W.; Chen, B.; Jiang, X.; et al. Effect of calcium addition in plasma catalysis for toluene removal by Ni/ZSM-5: acidity/basicity, catalytic activity and reaction mechanism. *J. Hazard. Mater.* **2020**, *387*, 122004. DOI
56. Dai, G.; Wang, K.; Wang, G.; Wang, S. Initial pyrolysis mechanism of cellulose revealed by in-situ DRIFT analysis and theoretical calculation. *Combust. Flame.* **2019**, *208*, 273-80. DOI
57. Leng, E.; Zhang, Y.; Peng, Y.; et al. In situ structural changes of crystalline and amorphous cellulose during slow pyrolysis at low temperatures. *Fuel* **2018**, *216*, 313-21. DOI
58. Wang, S.; Dai, G.; Ru, B.; et al. Influence of torrefaction on the characteristics and pyrolysis behavior of cellulose. *Energy* **2017**, *120*, 864-71. DOI
59. Agarwal, V.; Dauenhauer, P. J.; Huber, G. W.; Auerbach, S. M. Ab initio dynamics of cellulose pyrolysis: nascent decomposition pathways at 327 and 600 °C. *J. Am. Chem. Soc.* **2012**, *134*, 14958-72. DOI

Shuang Luo

Shuang Luo, a Ph.D. candidate at the School of Chemistry and Chemical Engineering, Chongqing University, conducts research on novel nanomaterials and porous materials for energy applications. Her research explores their potential in cutting-edge technologies such as solar energy conversion, photocatalysis, and thermocatalysis.

Min Mao

Min Mao is currently a postgraduate student in the School of Chemistry and Chemical Engineering, Chongqing University. Her research primarily focuses on low-dose transmission electron microscopy imaging techniques to investigate the structure-property relationship of beam-sensitive materials.

Haijie Yu

Haijie Yu, a doctoral student at Chongqing University, obtained his bachelor's and master's degrees from Chongqing University of Technology between 2014 and 2020. His research focuses on fundamental catalysis, with notable contributions in areas such as coal exhaust denitrification and selective oxidation of methane to produce oxygen-containing compounds.

Yuxin Zheng

Yuxin Zheng obtained her bachelor's degree from Chongqing University in 2022 and is currently pursuing a master's degree at the same institution. Her research primarily focuses on porous materials, heterogeneous catalysis, and photocatalytic degradation.

Zhaohui Liu

Dr. Zhaohui Liu received his Ph.D. in Chemical Science from King Abdullah University of Science and Technology in 2018 and subsequently worked as a postdoctoral fellow at the University of Delaware from 2018 to 2020. He joined Chongqing University in China in 2020, where he currently serves as an associate professor. His research primarily focuses on heterogeneous catalysis.

Lingmei Liu

Dr. Lingmei Liu is currently a Professor in Chongqing University, China. She earned her Ph.D. from the Institute of Metal Research, Chinese Academy of Science. From 2016 to 2019, she worked as a postdoctoral fellow in Prof. Yu Han's group at King Abdullah University of Science and Technology (KAUST), later serving as a research scientist in the same group until 2021. Her current research primarily focuses on electron microscopic study for beam-sensitive materials, including Metal-Organic Frameworks (MOFs), Covalent Organic Frameworks (COFs), and other crystalline porous materials. She has made significant contributions to the development and application of low-dose electron microscopy techniques for studying the high-resolution local structures of these materials without causing damage.

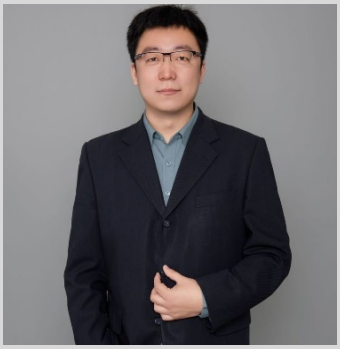

Jianjian Wang

Dr. Jianjian Wang is a distinguished researcher and doctoral supervisor at Chongqing University. He completed his undergraduate, master's, and doctoral degrees at East China University of Science and Technology in Shanghai between 2005 and 2014. From 2014 to 2016, he served as an assistant researcher at the Shanghai Advanced Research Institute of the Chinese Academy of Sciences. He then conducted postdoctoral research at King Abdullah University of Science and Technology in Saudi Arabia from 2016 to 2018, where he was later promoted to research scientist from 2018 to 2019. In February 2019, Dr. Wang joined Chongqing University under the "Young Hundred Talents Program".

To date, he has published over 60 academic papers in prestigious journals such as *Nat Chem*, *Nat Commun*, *J Am Chem Soc*, *Angew Chem Int Ed*, *Chem Mat*, *AIChE J*, *and Green Chem.* He has also led numerous projects funded by the National Natural Science Foundation of China, the Basic Research Fund for Central Universities, the Chongqing Natural Science Foundation, and various corporate collaborations.